UC Davis
UC Davis Previously Published Works

Title
Reaching 200-ps timing resolution in a time-of-flight and depth-of-interaction positron emission tomography detector using phosphor-coated crystals and high-density silicon photomultipliers

Permalink
https://escholarship.org/uc/item/8n3882b0

Journal
Journal of Medical Imaging, 3(4)

ISSN
2329-4302

Authors
Kwon, Sun Il
Ferri, Alessandro
Gola, Alberto
et al.

Publication Date
2016-11-23

DOI
10.1117/1.jmi.3.4.043501

Peer reviewed

eScholarship.org Powered by the California Digital Library
University of California

Journal of Medical Imaging

MedicalImaging.SPIEDigitalLibrary.org

Reaching 200-ps timing resolution in a time-of-flight and depth-of-interaction positron emission tomography detector using phosphor-coated crystals and high-density silicon photomultipliers

Sun Il Kwon
Alessandro Ferri
Alberto Gola
Eric Berg
Claudio Piemonte
Simon R. Cherry
Emilie Roncali

SPIE.

Sun Il Kwon, Alessandro Ferri, Alberto Gola, Eric Berg, Claudio Piemonte, Simon R. Cherry, Emilie Roncali, "Reaching 200-ps timing resolution in a time-of-flight and depth-of-interaction positron emission tomography detector using phosphor-coated crystals and high-density silicon photomultipliers," *J. Med. Imag.* **3**(4), 043501 (2016), doi: 10.1117/1.JMI.3.4.043501.

Reaching 200-ps timing resolution in a time-of-flight and depth-of-interaction positron emission tomography detector using phosphor-coated crystals and high-density silicon photomultipliers

Sun Il Kwon,[a,*] Alessandro Ferri,[b] Alberto Gola,[b] Eric Berg,[a] Claudio Piemonte,[b] Simon R. Cherry,[a] and Emilie Roncali[a]
[a]University of California Davis, Department of Biomedical Engineering, Davis, California 95616, United States
[b]Fondazione Bruno Kessler, via Sommarive 18, Trento, Italy

Abstract. Current research in the field of positron emission tomography (PET) focuses on improving the sensitivity of the scanner with thicker detectors, extended axial field-of-view, and time-of-flight (TOF) capability. These create the need for depth-of-interaction (DOI) encoding to correct parallax errors. We have proposed a method to encode DOI using phosphor-coated crystals. Our initial work using photomultiplier tubes (PMTs) demonstrated the possibilities of the proposed method, however, a major limitation of PMTs for this application is poor quantum efficiency in yellow light, corresponding to the wavelengths of the converted light by the phosphor coating. In contrast, the red-green-blue-high-density (RGB-HD) silicon photomultipliers (SiPMs) have a high photon detection efficiency across the visible spectrum. Excellent coincidence resolving time (CRT; <210 ps) was obtained by coupling RGB-HD SiPMs and $3 \times 3 \times 20$ mm^3 lutetium fine silicate crystals coated on a third of one of their lateral sides. Events were classified in three DOI bins (~6.7-mm width) with an average sensitivity of 83.1%. A CRT of ~200 ps combined with robust DOI encoding is a marked improvement in the phosphor-coated approach that we pioneered. For the first time, we read out these crystals with SiPMs and clearly demonstrated the potential of the RGB-HD SiPMs for this TOF-DOI PET detector. *© 2016 Society of Photo-Optical Instrumentation Engineers (SPIE)* [DOI: 10.1117/1.JMI.3.4.043501]

Keywords: positron emission tomography; depth-of-interaction; time-of-flight; phosphor coating; silicon photomultiplier; coincidence timing resolution.

Paper 16177R received Aug. 8, 2016; accepted for publication Oct. 28, 2016; published online Nov. 23, 2016.

1 Introduction

Positron emission tomography (PET) is one of the major clinical imaging modalities that provide functional images used to diagnose, stage, and monitor response to treatment in cancer, as well as to study neurodegenerative and cardiac-related diseases.[1,2] With the development of radiotracers, the use of PET has expanded to studying infectious diseases.[3–5] Current research in the field of clinical PET instrumentation focuses on increasing the sensitivity of PET scanners with thicker detectors, extended axial field-of-view (AFOV), and improved time-of-flight (TOF) capability in order to improve image signal-to-noise ratio (SNR). These improvements will allow for early detection of small cancer lesions, stem cells studies, and dose reduction in patients.[6–12] However, the use of thick detectors creates depth-of-interaction (DOI) parallax errors, which result in poorer spatial resolution and quantification near the edges of the FOV. To address this issue, many DOI-encoding strategies have been developed. Although the motivation for DOI encoding has traditionally been to reduce radial DOI blurring in small bore preclinical scanners, there is interest in developing clinical DOI-encoding detectors for a long AFOV scanner. In a long AFOV scanner, the wide acceptance angle may lead to considerable DOI blurring in the axial direction.[7,9] Along with this, as the achievable timing resolution continues to improve beyond 100 to 200 ps, the contribution of DOI-dependent photon transit times becomes nonnegligible. However, with sufficient DOI encoding, timing resolution can be improved by incorporating DOI information, although improvements in high-aspect ratio crystals are limited by the dispersion of the scintillation photons in this geometry. Overall, image SNR can be improved by using both TOF and DOI encoding information[13] and this motivates the development of detectors that simultaneously enable TOF and DOI encoding.

We have proposed a method to encode DOI using phosphor-coated crystals and pulse-shape discrimination techniques and recently investigated how this approach could be extended to TOF detectors.[14,15] Our initial work with these TOF-DOI detectors was performed with fast photomultiplier tubes (PMTs).[14] Using $4 \times 4 \times 20$ mm^3 lutetium oxyorthosilicate (LSO) crystals, we showed that DOI could be encoded at an acceptable 40-ps degradation of the timing resolution (~360 ps).[16] However, a major limitation of PMTs for this specific method is their low quantum efficiency (QE) at longer wavelengths (e.g., 10% or less at 540 nm), leading to poor detection efficiency for the phosphor-converted photons and ultimately resulting in suboptimal DOI and energy resolution compared to what could be obtained with a photodetector with higher QE at longer wavelengths.

*Address all correspondence to: Sun Il Kwon, E-mail: sunkwon@ucdavis.edu

2329-4302/2016/$25.00 © 2016 SPIE

With their compact size and high gain (comparable with conventional PMTs), silicon photomultipliers (SiPMs) are a promising alternative to PMTs for PET.[17] SiPMs are insensitive to magnetic field and provide excellent timing resolution.[17–19] Hence, SiPMs can be employed not only for preclinical PET scanners, but also for simultaneous PET/MRI clinical scanners, and TOF PET scanners.[20–23] Recently, SiPMs with high photon detection efficiency (PDE) were introduced by several companies. Some of these SiPMs adopted n-on-p structures and showed high PDE across a large region of the visible spectrum.[17] These are highly attractive for our phosphor-coated DOI detectors, since the phosphor coating not only modifies the temporal properties of detected scintillation light, but also shifts the light from blue (~430 nm) to yellow (~540 nm). It follows that use of a photodetector with high PDE both at short and longer wavelengths may contribute to improved energy, timing, and DOI-encoding performance with phosphor-coated crystals. Among these high PDE SiPMs, red-green-blue-high-density (RGB-HD) SiPMs developed by the Fondazione Bruno Kessler (FBK, Italy) showed excellent timing resolution due to low dark count noise and a fast signal response[24] and are a particularly suitable candidate for use in a combined TOF-DOI PET detector based on phosphor-coated crystals. By coupling phosphor-coated scintillation crystals to RGB-HD SiPMs, we can realize more of the benefits of our approach while addressing some of the limitations discovered in our previous studies using PMTs. Moreover, timing resolution can be much improved while preserving the DOI information. In this study, we evaluated the energy resolution, timing resolution, and DOI-encoding capability of TOF-DOI PET detectors made of $3 \times 3 \times 20$ mm^3 phosphor-coated crystals coupled to 4×4 mm^2 RGB-HD SiPMs.

2 Materials and Methods

2.1 *Scintillation Crystals and Phosphor-Coating*

The lutetium fine silicate (LFS) scintillation crystals used in this study have similar properties to LSO or lutetium–yttrium oxyorthosilicate (LYSO).[25–27] It was reported that LFS crystals have a slightly shorter decay time (35 ns) than LYSO and LSO, resulting in an improvement in timing resolution.[27] The shorter decay time is also an advantage for the depth-encoding method employed in this study.[28] Four polished $3 \times 3 \times 20$ mm^3 LFS pixels (Zecotek Photonics Inc., Canada) were prepared as shown in Fig. 1; for each crystal, a 7-mm-long section of one lateral side (3×20 mm^2) was coated with a ~100-μm-thick cerium-doped yttrium aluminum garnet (YAG:Ce, Comtech International Inc., Korea) phosphor.[29] The coating shape was optimized through previous simulation and experimental studies.[15,16,29] The portion of the crystals on which the coating was applied was roughly milled to ~100-μm depth prior to coating in order to maintain the original crystal pitch after the phosphor coating is applied to the crystal. This was done in anticipation of assembling crystal arrays (where it is ideal to use crystals with uniform cross section) and to improve the adhesion of the phosphor to crystals. The decay time of the YAG phosphor was measured to be 58 ns. The absorption spectrum of YAG matches very well with the emission spectrum of LFS crystals (peaked at 430 nm), while the emission spectrum is broad with a peak at 540 nm.[29]

When scintillation photons are generated in the crystal, some are absorbed and re-emitted by the phosphor, resulting in changes in the spectral and temporal properties of detected scintillation photons. By varying the coating in a depth-dependent manner, the fraction of the scintillation photons that interacts with the phosphor also varies in a depth-dependent manner. DOI can, therefore, be estimated by applying a suitable pulse discrimination technique to the scintillation pulses.[30] Two identical polished $3 \times 3 \times 5$ mm^3 LFS pixels were also prepared and used as a reference detector in coincidence timing experiments and to provide electronic collimation for fixed-depth irradiation to measure DOI encoding. All crystals were wrapped in five layers of polytetrafluoroethylene tape (Teflon tape) that has a reflectivity of ~97%.

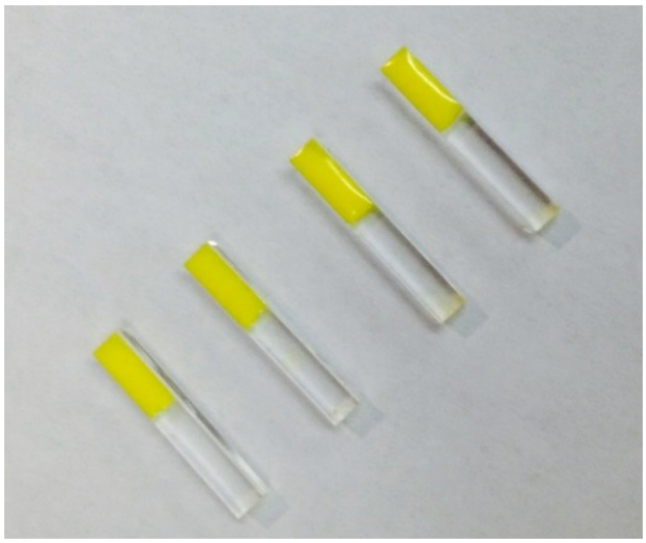

Fig. 1 YAG:Ce phosphor-coated LFS crystals with a size of $3 \times 3 \times 20$ mm^3. One lateral side of each LFS crystal was coated on a third of its length with a ~100-μm-thick layer of phosphor.

2.2 *Red-Blue-Green-High-Density Silicon Photomultipliers*

The latest generation RGB-HD SiPMs developed by FBK with a sensitive area of 4×4 mm^2 were used for energy, timing resolution, and DOI evaluation. The RGB-HD SiPMs combine the HD cell technology with the RGB SiPM[31] and exhibit extended PDE in the visible range compared to PMTs (Fig. 2). The HD technology features a reduced cell border width and allows the PDE to be close to 50%. The RGB-HD SiPMs used in this study have a cell pitch of 25 μm and a fill factor of ~70%. A protective silicone resin with excellent transparency for visible and near-UV light (down to 300 nm) was applied on the sensitive area of the RGB-HD SiPMs to protect bonding wires.

2.3 *Coincidence Measurement Setup*

Coincidence events from a ^{22}Na radioactive point source were recorded to evaluate the energy resolution, timing resolution, and DOI encoding [Fig. 3(a)]. Two identical SiPMs were selected based on their $I - V$ curves and connected to two transimpedance amplifiers. Each amplifier had two outputs: a slow output with a gain of ~100 V/A used to calculate the energy and pulse shape of each event, and a fast output with a pole-zero cancellation filter used to calculate coincidence resolving times (CRTs).[32] The rise time of the timing output was measured to be ~600 ps (from 10% to 90% of the signal amplitude). Output signals were digitized with an oscilloscope (DPO

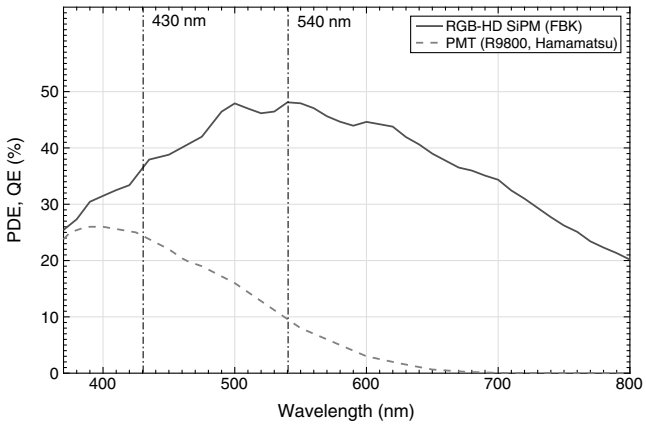

Fig. 2 QE of PMT (R9800, Hamamatsu) and PDE of RGB-HD SiPM (25 μm) measured at an overvoltage of 9 V. Dotted vertical lines show LFS (430 nm) and YAG:Ce (540 nm) emission peaks, respectively.

7254, Tektronix) at a sampling rate of 10 GS/s. Each energy signal was actively split into two signals using a linear fan-in-fan-out module (PS740, Phillips Scientific), where one copy of each signal is sent to an oscilloscope input channel while the second copy is passed through a leading edge discriminator (PS708, Phillips Scientific) and used for coincidence detection using a coincidence logic unit (PS756, Phillips Scientific). The timing signals from the amplifiers were directly coupled to input channels in the oscilloscope to prevent performance degradation and additional electrical noise.

The SiPM optimal bias voltage was determined using two identical detectors in coincidence. Each detector was composed of a $3 \times 3 \times 5$ mm^3 LFS crystal coupled to a 4×4 mm^2 SiPM. One of these detectors was then used as a reference detector for coincidence timing measurements with the phosphor-coated crystals. All four $3 \times 3 \times 20$ mm^3 LFS crystals were evaluated with the same SiPM before and after coating with YAG:Ce phosphor. Optical glue (Meltmount, Cargille Labs) with an index of refraction of 1.582 was used to couple the crystals to the SiPM.

Head-on measurements [Fig. 3(b)] were first performed, followed by side-on measurements [Fig. 3(c)] using electronic collimation[14,33,34] with a 0.5-mm diameter ^{22}Na point source (7.4 MBq) to evaluate the effect of DOI on the signals. The crystals were secured to the SiPMs using custom three-dimensional printed holders. Six thousand events were acquired in each measurement. The estimated width of the collimating beam at the crystal was 1.5 mm. Coincidence events at three different depth positions (2, 10, and 18 mm from the SiPM face) were acquired. The temperature of the detectors was maintained at 20°C by supplying chilled air into the holders.

2.4 *Energy and Timing Resolution*

Energy signals were integrated with a 1-μs time window and the resulting waveform sum values were histogrammed to form the energy spectrum. The 511-keV photopeak was fitted with a Gaussian distribution to compute the full width at half maximum (FWHM). The energy resolution was obtained by the ratio of the FWHM to the photopeak position. Saturation correction was not applied for the energy resolution results. Only coincidence events within the energy window (photopeak $\pm\, 0.5 \times$ FWHM) were used to measure the timing resolution, the decay time, and the DOI performance. For each coincidence event, the time pick-offs were obtained by leading edge thresholding after linear interpolation of the timing signals produced by each detector. The time difference between the two time pick-offs was computed for each of the coincidence events and the collection of time difference values was histogrammed to form the timing spectrum. The CRT was calculated as the FWHM of a Gaussian fit to the timing spectrum. A range of leading edge thresholds was compared for each dataset (each crystal, depth, and coating) and CRT as a function of leading edge threshold was computed for each configuration. The best CRT was then selected as a representative value of the processed dataset. The reference detector's intrinsic timing resolution was calculated from two identical detectors consisting of $3 \times 3 \times 5$ mm^3 LFS and SiPMs. Its contribution was subtracted in quadrature from the coincidence timing resolution values and the expected CRT ($=\sqrt{2} \times$ single detector timing resolution) is reported.[14,35]

2.5 *Depth-of-Interaction Positioning*

Depth-dependent variations in the pulse shapes were first qualitatively assessed using the decay times. The decay time was estimated as the time constant of a single exponential fit to the data.

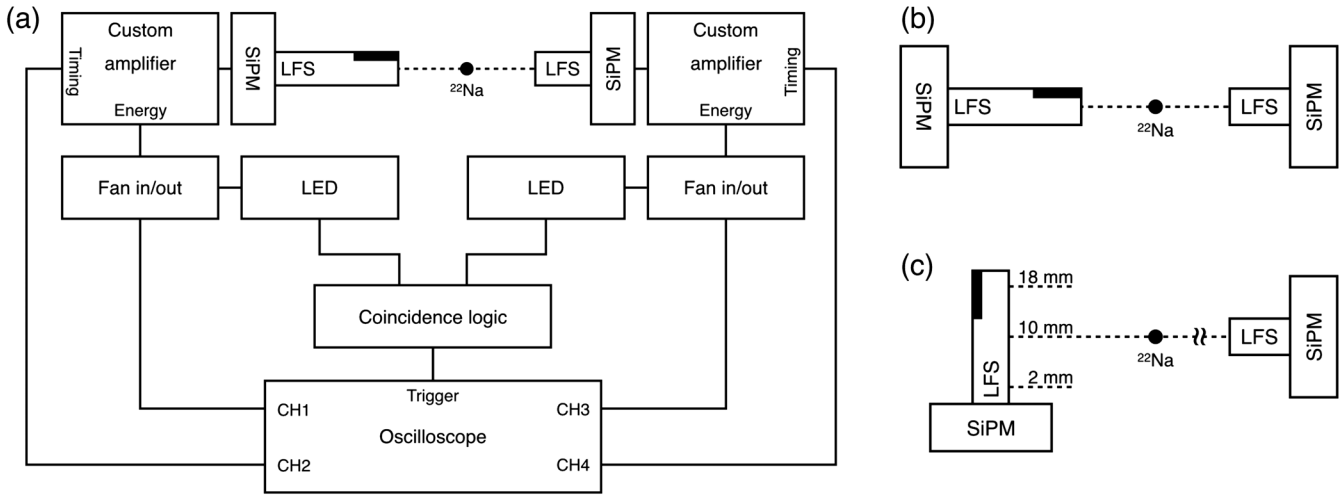

Fig. 3 (a) Experimental setup for coincidence events measurements, (b) head-on, and (c) side-on measurements configurations.

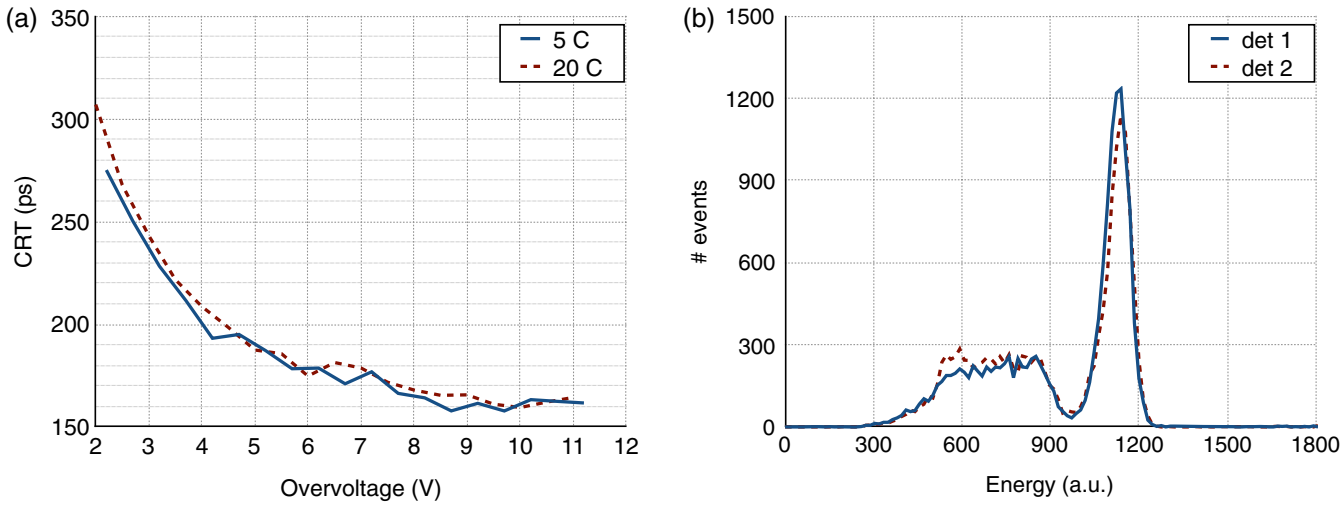

Fig. 4 CRT as a function of (a) overvoltage and (b) energy spectra of two reference detectors, each consisting of an uncoated $3 \times 3 \times 5$ mm^3 LFS crystal and an RGB-HD SiPM.

The average decay time was calculated for each known irradiation depth and provided an estimation of the DOI-encoding performance. Quantitative DOI encoding was then computed using delayed charge integration (DCI), a more robust and superior approach that we have investigated in previous studies.[33] In the DCI method, each pulse was integrated over two sequential time windows, each of 200-ns width and a delay of 90 ns. The ratio of these two integrals describes the amount of light contained in the early and late parts of the signal and thus provides a unique pulse-shape signature for each pulse. DCI values were used to classify the pulses in three DOI bins using linear discriminant analysis. To characterize the performance of the DOI encoding, DOIs predicted by the classifier were histogrammed for each DOI bin (2, 10, and 18 mm). The classification sensitivity per bin, defined as the ratio of correctly assigned events to the total number of events and expressed as a percentage, was calculated for each irradiation depth.

3 Results

3.1 *Coincidence Measurements using Two Short Lutetium Fine Silicate Crystals*

We first optimized the SiPM bias voltage using the reference detectors (two $3 \times 3 \times 5$ mm^3 LFS crystals coupled to the SiPMs) and acquiring coincidence data with a ^{22}Na point source. Measurements were taken at 5°C and 20°C. Optical grease (BC-630, Saint-Gobain) was applied in this experiment only. Figure 4(a) shows CRT values as a function of overvoltage (defined as applied bias voltage—breakdown voltage).[17] The CRT decreased rapidly with increasing overvoltage and reached a stable minimum value of ~160 ps at 9.5 V overvoltage 20°C. CRT measured at 5°C showed slightly better results than those at 20°C. Both SiPMs showed very similar gains at the same bias voltage (9.5 V), as determined from the overlapping energy spectra [Fig. 4(b)]. An overvoltage of 9.5 V and temperature of 20°C were applied in all subsequent experiments.

We observed in these experiments that the photopeak position decreased and CRT degraded by ~7 ps shortly after coupling the crystals to SiPMs with optical grease (~30 min). This was due to the optical grease penetrating into the Teflon tape and the evaporation of optical grease due to the chilled, dry air used in our cooling system. After the initial degradation, the CRT remained stable for up to 16 h after crystal coupling. We used Meltmount in all subsequent experiments to overcome this issue and obtain stable timing performance in the reference detector. The best CRT achieved was 150 ps, which translates to an intrinsic timing resolution of 106 ps for the reference detector.

3.2 *Head-On Measurements*

Photopeak position, energy resolution, and expected CRT (after correcting for the reference detector contribution) in the head-on measurement were computed using four $3 \times 3 \times 20$ mm^3 LFS crystals both before and after coating (Table 1). Photopeak positions were slightly lower with the coated crystals (~3% decrease). When applying the coating, the energy resolution degraded by 3.7% while the coincidence timing resolution degraded by 23 ps. Variations (measured as the standard deviation using the values obtained with the four crystals) of the photopeak position and the energy resolution increased slightly after coating, while the intercrystal variation of timing resolution was not affected by the coating.

3.3 *Side-On Measurements*

Figure 5 shows the histogram of the decay times for each irradiation depth obtained by fitting the pulse from each individual event. Decay times of uncoated crystals coupled to SiPMs did not vary with depth [Fig. 5(a)]. The average decay times of uncoated crystals irradiated at depths of 2, 10, and 18 mm

Table 1 Results from head-on measurements using four LFS crystals before (uncoated) and after (coated) coating.

	Uncoated	Coated
Photopeak position	1892 ± 37	1830 ± 115
Energy resolution	$9.4 \pm 0.47\%$	$13.2 \pm 2.71\%$
Expected CRT	186 ± 8.5 ps	209 ± 7.0 ps

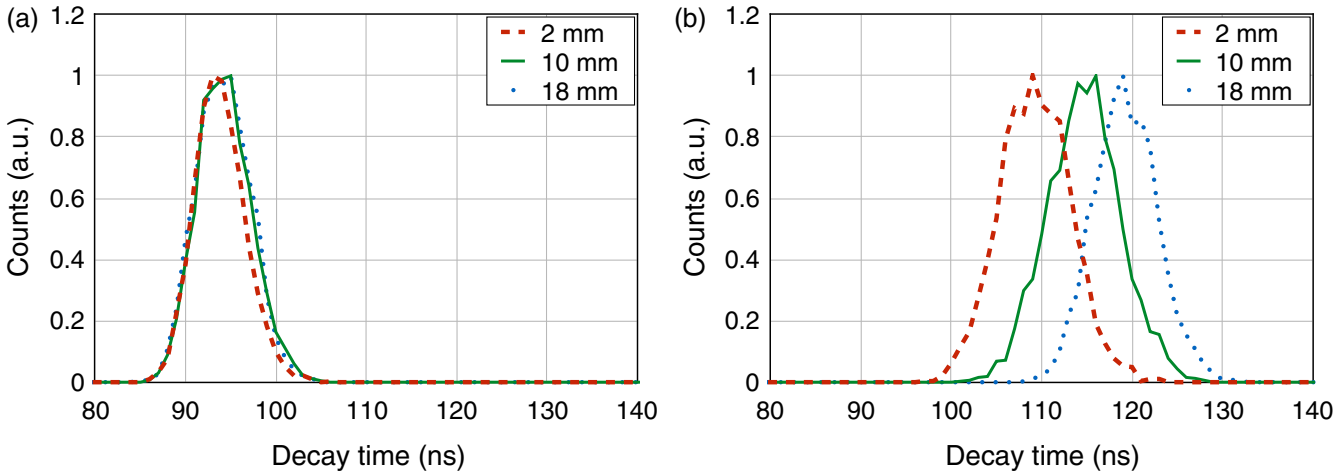

Fig. 5 Decay time histograms of (a) uncoated and (b) coated LFS crystals at irradiation depths of 2, 10, and 18 mm.

were 94 ± 2.8, 94 ± 3.0, and 94 ± 3.0 ns, respectively. The measured decay time of pulses from uncoated LFS crystals coupled to SiPMs was longer than that of the intrinsic decay time of LFS crystals (35 ns) due to convolution with the SiPM and electronics response time. On the contrary, for the coated crystals, pulses acquired at 18 mm had a higher fraction of converted light because of the phosphor coating, leading to a longer measured decay time with increasing depth. The average decay times of coated crystals at 2, 10, and 18 mm irradiation depths were 109 ± 3.9, 115 ± 4.0, and 119 ± 3.5 ns, respectively, [Fig. 5(b)].

DOI-dependent changes in photopeak position, energy resolution, and the expected CRT of LFS crystals are shown in Fig. 6. The values and uncertainties in Fig. 6 represent the average and standard deviation across the four crystals, respectively. For the original uncoated crystals (Fig. 6, light bars), the photopeak position of the uncoated LFS crystals decreased by 3.8% with increasing depth (from 2 to 18 mm). The CRT at 10-mm depth was slightly worse (8 ps) than that at 2 and 18 mm [Fig. 6(c)]. Overall, the depth-dependent variations with uncoated crystals were negligible.

In contrast, coated LFS crystals showed depth-dependent variations in all performance metrics (Fig. 6, dark bars). The trend of photopeak position versus DOI was reversed with phosphor-coated crystals compared to uncoated crystals, as the photopeak position increased from 2- to 18-mm DOI. This is likely due to the higher PDE of RGB-HD SiPMs at 540 versus 430 nm, which favors the collection of the converted light over nonconverted light. Energy resolution with the coated crystals worsened slightly with increasing depth. Timing resolution showed small degradations (<25 ps) at 2- and 10-mm depths compared to uncoated crystals, while the timing resolution of coated crystals at 18-mm depth was comparable with that of uncoated crystals. This may be due to the roughening of the crystal surface prior to coating with the phosphor that tends to improve the timing resolution.[36]

For the CRT measurements, the optimal leading edge threshold that was determined did not vary strongly between coated and uncoated crystals or with depth. In most cases, the best CTR values were obtained at leading edge thresholds between 6 and 10 mV.

3.4 *Depth-of-Interaction Classification*

Figure 7 shows the fraction of events classified in each DOI bin as a function of DOI with phosphor-coated crystals. For all histograms, the horizontal axis shows the known DOI bin centers and the vertical axis shows the fraction of events assigned to those bins. Labels on the left of the plots indicate the true irradiation depth. Black bars indicate the correct DOI bin. Coated crystals showed excellent classification sensitivity with an average of 83.1% pulses correctly classified (88.0% at 2mm, 75.7% at 10 mm, and 85.5% at 18 mm). This demonstrates the capability of our TOF-DOI detector to encode reasonable DOI information, while preserving the timing resolution.

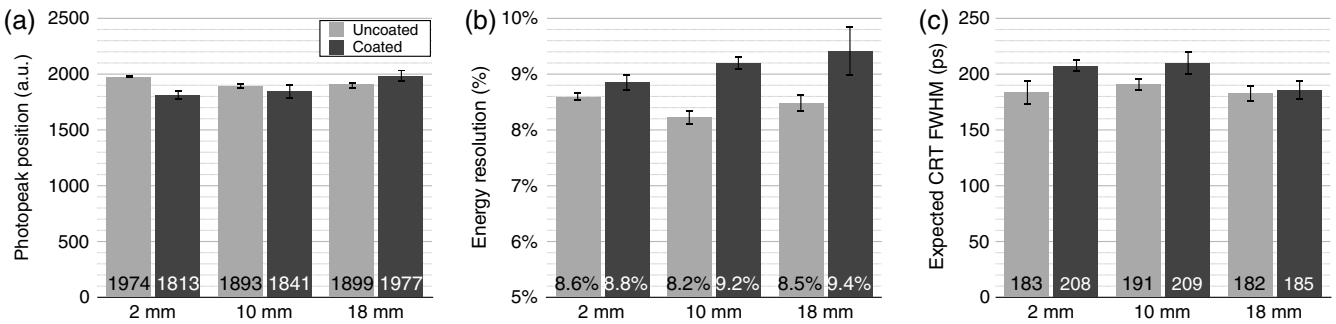

Fig. 6 Measurements of (a) 511-keV photopeak position, (b) energy resolution, and (c) expected CRT at irradiation depths of 2, 10, and 18 mm with LFS crystals before (gray bars) and after (black bars) coating using the side-on configuration.

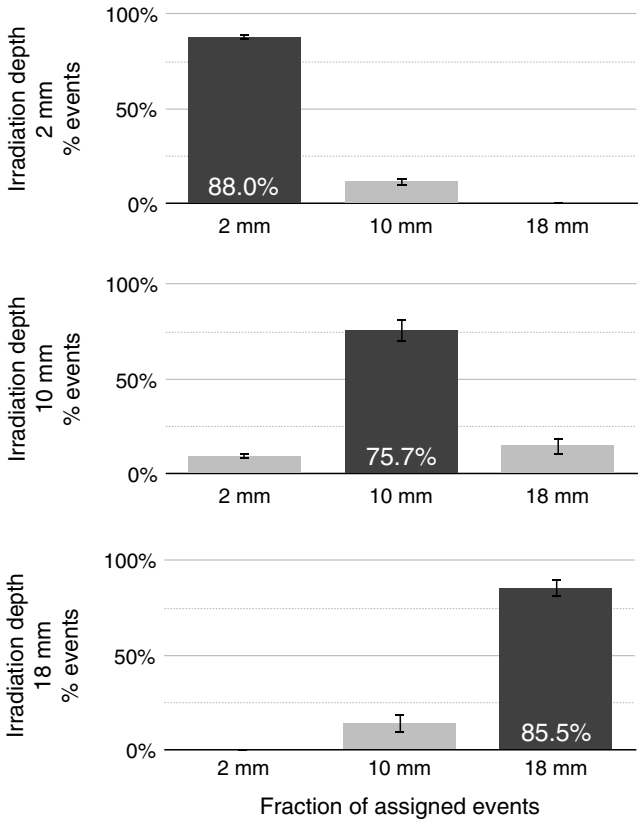

Fig. 7 DOI classification results. Black bar indicates the correct depth.

4 Discussion and Conclusions

We characterized the performance of TOF-DOI PET detectors using phosphor-coated LFS crystals directly coupled to RGB-HD SiPMs. Excellent timing resolution (<210 ps) was obtained with single $3 \times 3 \times 20$ mm^3 coated LFS crystals in both head-on and side-on measurements. Only a slight degradation in timing resolution (<25 ps) was observed with phosphor-coated crystals compared to uncoated crystals. Consistent with results from other groups, the timing resolution slightly improved at lower temperatures; however, the improvement was small.[24,37,38] Maintaining a stable temperature of less than 10°C requires a more complex cooling system that increases the cost of a complete scanner. The small improvement in timing resolution observed with a decrease in temperature in our detectors (<10 ps between 5°C and 20°C) is not sufficient to justify this additional cost, as a timing resolution of 210 ps at 20°C would already result in significant improvement of the scanner SNR.[8,11,39] The gain in timing resolution without losing DOI-encoding accuracy was attributable to the high PDE of the RGB-HD SiPMs across the visible spectrum and the low dark count.[31,38] We also hypothesize that for scintillation events occurring near the phosphor-coated region (i.e., away from the SiPM), the pool of early visible photons used for time pick-off may include phosphor-converted photons. Therefore, a higher PDE in the yellow may further improve the timing resolution with phosphor-coated crystals. We will use Monte Carlo simulation studies to test this hypothesis in future work.

In general, light collection (photopeak position) in a long, narrow crystal decreases with increasing DOI due to increased self-absorption in the crystal and light loss at interfaces between lateral surfaces of the crystal and the wrapping material.[40,41] In our previous studies with phosphor-coated crystals coupled to PMTs,[14] the photopeak position showed stronger depth dependency as a result of the low PMT QE for converted light by the phosphor. On the contrary, here the photopeak position with coated crystals increased sharply between 10 and 18 mm due to the higher PDE of the RGB-HD SiPMs at ~540 nm (the peak emission wavelength of YAG) than at ~420 nm (the peak emission wavelength of LFS). This is important because in 20-mm-thick detectors the majority of events occur in the entrance half of the crystal where the coating is applied, i.e., where there is now a large gradient in light collection. Indeed, this affected energy resolution of the coated crystals in head-on measurements; the energy resolution of a coated crystal was much worse than that of an uncoated crystal (Table 1) due to the gradient in light collection in the entrance half of the crystal. To counteract the depth-dependent effects, head-on events were classified into the three DOI bins based on their DCI values. Approximately 60% of head-on coincidence events were classified to the third bin (close to the entrance surface of a crystal). Energy resolution was computed for each set of classified events, leading to a DOI-corrected average head-on energy resolution of 10.8%, a considerable improvement from the original energy resolution of 13.2% (Table 1). The CRTs of coincidence events classified in the third and second bins from head-on data were 185 and 211 ps, respectively, while the average expected CRTs without depth-encoding was 209 ps (Table 1). These average CRTs showed good agreement with side-on measurements [Fig. 6(c)].

We demonstrated robust DOI encoding with classifying events into three DOI bins; our future work will focus on evaluating the DOI performance using a finer DOI binning. Here, we used a DCI-based classification method that is known to work well but we will evaluate other pulse-shape discrimination techniques that have shown improved DOI encoding with PMTs.[28]

Acknowledgments

This work was funded by the UC Davis Research Investment in Science and Engineering Program and NIH Grants Nos. R01 EB019439 and R01 CA206187. The authors have nothing to disclose and want to thank Steven Lucero in University of California, Davis, for useful discussions.

References

1. P. Edison et al., "Amyloid, hypometabolism, and cognition in Alzheimer disease: an [11C]PIB and [18F]FDG PET study," *Neurology* **68**(7), 501–508 (2007).
2. A. Martinez-Moller et al., "Dual cardiac-respiratory gated PET: implementation and results from a feasibility study," *Eur. J. Nucl. Med. Mol. Imaging* **34**(9), 1447–1454 (2007).
3. A. W. Glaudemans and A. Signore, "FDG-PET/CT in infections: the imaging method of choice?," *Eur. J. Nucl. Med. Mol. Imaging* **37**(10), 1986–1991 (2010).
4. G. Gowrishankar et al., "Investigation of 6-[18F]-fluoromaltose as a novel PET tracer for imaging bacterial infection," *PLoS One* **9**(9), e107951 (2014).
5. X. Wang and N. Murthy, "Bacterial imaging comes of age," *Sci. Transl. Med.* **6**(259), 1–3 (2014).
6. J. V. Frangioni and R. J. Hajjar, "In vivo tracking of stem cells for clinical trials in cardiovascular disease," *Circulation* **110**(21), 3378–3383 (2004).
7. S. R. Cherry, "The 2006 Henry N. Wagner lecture: of mice and men (and positrons)-advances in PET imaging technology," *J. Nucl. Med.* **47**(11), 1735–1745 (2006).

8. J. S. Karp et al., "Benefit of time-of-flight in PET: experimental and clinical results," *J. Nucl. Med.* **49**(3), 462–470 (2008).
9. J. K. Poon et al., "Optimal whole-body PET scanner configurations for different volumes of LSO scintillator: a simulation study," *Phys. Med. Biol.* **57**(13), 4077–4094 (2012).
10. S. Gaedicke et al., "Noninvasive positron emission tomography and fluorescence imaging of CD133+ tumor stem cells," *Proc. Natl. Acad. Sci. U. S. A.* **111**(6), 692–701 (2014).
11. S. Surti, "Update on time-of-flight PET imaging," *J. Nucl. Med.* **56**(1), 98–105 (2015).
12. G. A. Ulaner et al., "Prognostic value of FDG PET/CT before allogeneic and autologous stem cell transplantation for aggressive lymphoma," *Radiology* **277**(2), 518–526 (2015).
13. H. Thoen et al., "Influence of detector parameters on lesion detectability for PET scanners with long axial FOV," *J. Nucl. Med.* **55**(Suppl. 1), 2153 (2014).
14. J. P. Schmall et al., "Timing properties of phosphor-coated polished LSO crystals," *Phys. Med. Biol.* **59**(15), N139 (2014).
15. E. Roncali et al., "Predicting the timing properties of phosphor-coated scintillators using Monte Carlo light transport simulation," *Phys. Med. Biol.* **59**(8), 2023–2039 (2014).
16. E. Berg et al., "A combined time-of-flight and depth-of-interaction detector for total-body positron emission tomography," *Med. Phys.* **43**(2), 939–950 (2016).
17. E. Roncali and S. R. Cherry, "Application of silicon photomultipliers to positron emission tomography," *Ann. Biomed. Eng.* **39**(4), 1358–1377 (2011).
18. S. J. Hong et al., "An investigation into the use of Geiger-mode solid-state photomultipliers for simultaneous PET and MRI acquisition," *IEEE Trans. Nucl. Sci.* **55**(3), 882–888 (2008).
19. D. R. Schaart et al., "$LaBr_3$: Ce and SiPMs for time-of-flight PET: achieving 100 ps coincidence resolving time," *Phys. Med. Biol.* **55**(7), N179 (2010).
20. S. Yamamoto et al., "Development of a Si-PM-based high-resolution PET system for small animals," *Phys. Med. Biol.* **55**(19), 5817–5831 (2010).
21. S. I. Kwon et al., "Development of small-animal PET prototype using silicon photomultiplier (SiPM): initial results of phantom and animal imaging studies," *J. Nucl. Med.* **52**(4), 572–579 (2011).
22. H. S. Yoon et al., "Initial results of simultaneous PET/MRI experiments with an MRI-compatible silicon photomultiplier PET scanner," *J. Nucl. Med.* **53**(4), 608–614 (2012).
23. M. A. Queiroz et al., "Dose optimization in TOF-PET/MR compared to TOF-PET/CT," *PLoS One* **10**(7), e0128842 (2015).
24. M. V. Nemallapudi et al., "Sub-100 ps coincidence time resolution for positron emission tomography with LSO:Ce codoped with Ca," *Phys. Med. Biol.* **60**(12), 4635–4649 (2015).
25. T. K. Lewellen et al., "Initial evaluation of the scintillator LFS for positron emission tomograph applications," in *IEEE Nuclear Science Symp. Conf. Record*, pp. 2915–2918 (2004).
26. M. Grodzicka et al., "Characterization of LFS-3 scintillator in comparison with LSO," *Nucl. Instrum. Methods Phys. Res. Sect. A* **652**(1), 226–230 (2011).
27. K. Doroud et al., "Comparative timing measurements of LYSO and LFS-3 to achieve the best time resolution for TOF-PET," *Nucl. Instrum. Methods A* **793**, 57–61 (2015).
28. E. Berg et al., "Improving depth, energy and timing estimation in PET detectors with deconvolution and maximum likelihood pulse shape discrimination," *IEEE Trans. Med. Imaging* **35**(11), 2436–2446 (2016).
29. E. Roncali, V. Viswanath, and S. R. Cherry, "Design considerations for DOI-encoding PET detectors using phosphor-coated crystals," *IEEE Trans. Nucl. Sci.* **61**(1), 67–73 (2014).
30. H. Du et al., "Continuous depth-of-interaction encoding using phosphor-coated scintillators," *Phys. Med. Biol.* **54**(6), 1757–1771 (2009).
31. C. Piemonte et al., "Characterization of the first FBK high-density cell silicon photomultiplier technology," *IEEE Trans. Electron Devices* **60**(8), 2567–2573 (2013).
32. A. Gola, C. Piemonte, and A. Tarolli, "Analog circuit for timing measurements with large area SiPMs coupled to LYSO crystals," *IEEE Trans. Nucl. Sci.* **60**(2), 1296–1302 (2013).
33. E. Roncali et al., "Pulse shape discrimination and classification methods for continuous depth of interaction encoding PET detectors," *Phys. Med. Biol.* **57**(20), 6571–6585 (2012).
34. M. S. Brown et al., "Influence of depth of interaction upon the performance of scintillator detectors," *Proc. Natl. Acad. Sci. U. S. A.* **9**(5), e98177 (2014).
35. M. Ito, L. Jin Pyo, and L. Jae Sung, "Timing performance study of new fast PMTs with LYSO for time-of-flight PET," *IEEE Trans. Nucl. Sci.* **60**(1), 30–37 (2013).
36. E. Berg, E. Roncali, and S. R. Cherry, "Optimizing light transport in scintillation crystals for time-of-flight PET: an experimental and optical Monte Carlo simulation study," *Biomed. Opt. Express* **6**(6), 2220–2230 (2015).
37. V. Puill et al., "Single photoelectron timing resolution of SiPM as a function of the bias voltage, the wavelength and the temperature," *Nucl. Instrum. Methods Phys. Res. Sect. A* **695**, 354–358 (2012).
38. A. Ferri et al., "Performance of FBK high-density SiPM technology coupled to Ce:LYSO and Ce:GAGG for TOF-PET," *Phys. Med. Biol.* **59**(4), 869–880 (2014).
39. D. J. Kadrmas et al., "Impact of time-of-flight on PET tumor detection," *J. Nucl. Med.* **50**(8), 1315–1323 (2009).
40. V. C. Spanoudaki and C. S. Levin, "Investigating the temporal resolution limits of scintillation detection from pixellated elements: comparison between experiment and simulation," *Phys. Med. Biol.* **56**(3), 735–756 (2011).
41. J. Y. Yeom, R. Vinke, and C. S. Levin, "Optimizing timing performance of silicon photomultiplier-based scintillation detectors," *Phys. Med. Biol.* **58**(4), 1207–1220 (2013).

Sun Il Kwon received his PhD from Seoul National University and is currently an assistant project scientist at the University of California, Davis. His research is focused on the development of positron emission tomography (PET) instrumentation including scintillators, photosensors, electronics, and system design.

Alessandro Ferri received his Laurea degree in physics from the University of Bologna, Italy, in 2011. Since 2011, he has been with the Fondazione Bruno Kessler (FBK), Trento, Italy, where he is currently a junior researcher. His activity is focused on the characterization of silicon photomultipliers (SiPMs).

Alberto Gola received his MS degree in electronic engineering and his PhD in information technology from Politecnico di Milano, Milano, Italy, in 2003 and 2007, respectively. Since 2010, he has been with the FBK, Trento, Italy, where he is currently a junior researcher. His activity is focused on the development of SiPMs.

Eric Berg is a postdoctoral scholar of biomedical engineering at University of California, Davis, with research focus on detector and scanner technology for total-body PET imaging.

Claudio Piemonte received his MS (Laurea) degree in electronic engineering from the University of Trieste, Italy, in 1997. Since 2002, he has been with the FBK, Trento, Italy, where he is currently a chief scientist of the Radiation Detection and Imaging Research Line.

Simon R. Cherry has a background in physics and is currently a professor of biomedical engineering and radiology at the University of California, Davis. His research is focused on developing imaging technologies, methods, and systems for molecular imaging. He is a member of the National Academy of Engineering.

Emilie Roncali obtained her PhD from the French Atomic Energy Commission, investigating luminescence imaging for preclinical applications. She is a scientist at the University of California, Davis, and an IEEE senior member. Her current research interests involve the design of detectors for PET, Monte Carlo simulation with an emphasis on light transport, implementation of optical models in Monte Carlo packages (e.g., GATE), and quantitative simulation for dosimetry applications in radiotherapy.